UDC 629.705(045)
DOI:10.18372/1990-5548.88.20979

[1]Vadym Avrutov,
[2]Oleksii Hehelskyi,
[3]Viacheslav Tsisarzh,
[4]Olha Pazdrii
[5]Maksym Khutko

MODAL CONTROL OF UNMANNED AERIAL VEHICLE ROLL ANGLE

[1,2,4,5]National Technical University of Ukraine "Ihor Sikorsky Kyiv Polytechnic Institute," Kyiv, Ukraine
[3]State Enterprise "Research Institute "Kvant-Radiolokatsiia", Kyiv, Ukraine
E-mails: [1]vyshgorod@gmail.com ORCID 0000-0002-3875-0646,
[2]hehelskyi.oleksii@gmail.com ORCID 0000-0002-8108-4730,
[3]tsisarzh_v@ukr.net ORCID 0009-0004-3294-2710
[4]olgapazdri@gmail.com ORCID 0000-0002-8970-5079
[5]khutko.m.yu.-pg51f@edu.kpi.ua ORCID 0009-0006-8344-6674

Abstract*—The article deals with the problem of automatic control of the roll angle of an unmanned aerial vehicle. Based on the complete mathematical model of the unmanned aerial vehicle and modal control methods, two variants of the automatic control system are considered: an autopilot implemented as a closed-loop feedback system and a system with an observer device. The controllability and observability conditions of the system are analyzed, and the autopilot equation with a structure corresponding to a PID controller is obtained. Numerical simulation results are presented in the form of time dependences of the roll angle, roll rate, and aileron deflection angle for different natural frequencies. Analytical verification confirms the steady-state value of the roll angle obtained by simulation. The parameters of the autopilot for different transient processes are determined. The roots of the characteristic equations for the binomial and Butterworth standard forms are calculated, and analytical expressions for the gain matrix of the Luenberger observer are obtained. The results show that the use of an observer device significantly changes the transient response of the system. The proposed approach based on modal control methods can be applied not only to roll control but also to the design of automatic control systems for pitch and yaw angles of unmanned aerial vehicles and other aircraft.*

Keywords—Autopilot, observer, automatic control system, roll angle, unmanned aerial vehicle, PID controller.

I. INTRODUCTION

Today, unmanned aerial vehicles (UAVs) perform a very wide range of tasks across various fields – from military operations to cinematography. The role of UAVs on the battlefield is rapidly growing. UAVs used in modern warfare have completely transformed military tactics by offering unique operational advantages and improving efficiency across various combat scenarios [1]. Each UAV contains multiple automatic control systems (ACS): for fuel management and power consumption, communication, navigation and orientation autopilots, and electro-optical video-surveillance systems. The autopilot subsystem includes platform-free inertial navigation systems integrated with satellite navigation, barometric altitude sensors, and air data receivers. Therefore, improving flight control systems remains a highly relevant scientific and engineering challenge. Numerous studies have examined the development and improvement of UAV control systems.

In article [2], flight control of a novel tiltrotor aircraft is considered. This type of aerial vehicle has two flight modes and one transitional mode. During the vertical take-off and landing phase, the aircraft operates as a quadrotor helicopter, while during the horizontal flight phase, it functions as a conventional airplane. The transitional mode lies between these two flight states. In that work, a new tiltrotor aircraft was introduced, where the transition is achieved by dual forward tilting, and a corresponding mathematical model was developed. During vertical take-off and landing, a classical PID-controller method was applied, and numerical simulations confirmed good control performance. To ensure a stable transition between vertical and horizontal flight, a nonlinear control law based on the backstepping method was proposed. The results demonstrated that a stable mode transition can be achieved, confirming the effectiveness of the

proposed control approach. Finally, vertical flight experiments were carried out on the newly designed aircraft.

A multimodal UAV configuration was proposed in [3], combining a tail-sitter arrangement with an integrated channelized wing design. The tail-sitter and semi-ducted structures complement each other, improving UAV maneuverability, transition speed, stability, and reliability during vertical-to- horizontal transitions. The configuration also supports short-takeoff-and-landing and vertical-takeoff-and-landing modes, significantly expanding its operational scope. For the transition phase, full-modal control rules based on complementary filtering and fixed-point target coordinate control were developed. These rules allow the avoidance of complex logic switching, making the control system smoother and more concise. Simulation and flight test results confirmed the feasibility of the proposed design.

The use of UAVs as aerial base stations has attracted increasing scientific attention in recent years [4]. The key challenge in this field is the deployment of multiple UAVs in dynamic environments, especially where user demands change over time. To address this, an adaptive UAV deployment scheme in dynamic wireless networks was proposed, considering the mobility of UAVs and users, state variability, and adjustable UAV transmission power. Through joint optimization of UAV operating modes, transmission power levels, and movement strategies, the goal is to balance energy consumption minimization and ground-user coverage maximization. A deep reinforcement-learning-based approach was adopted. To capture dynamic variations of users and UAVs in the environment, a multimodal state-feature space was developed, combining multi-channel image data and vector representations. The image component integrates user distribution and real-time UAV coverage, while the vector component encodes UAV operating modes, location, and temporal system information. These multimodal features are processed through convolutional neural networks (CNN) and multilayer perceptrons for enhanced feature extraction. To improve training stability and efficiency, parameter updates are performed using the proximal policy optimization method. Simulation results demonstrate the effectiveness of the proposed approach in balancing energy consumption and coverage while efficiently managing system dynamics.

The development of computer-vision algorithms for UAV imagery largely depends on the availability of annotated high-resolution aerial datasets [5]. However, the scarcity of large-scale real datasets with pixel-level annotations poses a significant challenge, as limited image counts in existing datasets hinder the performance of deep-learning models that require extensive training data. To overcome this limitation, a multimodal synthetic dataset containing both images and 3D data captured at various flight altitudes was proposed. In addition to object-level annotations, pixel-level labels for 28 semantic classes were included, enabling research in tasks such as semantic segmentation. The dataset contains over 72,000 labeled samples, enabling efficient training of deep architectures and showing promising results in synthetic-to-real domain adaptation. The dataset will be made publicly available to support further computer-vision research focused on UAV applications.

A new dynamic photogrammetry method using UAVs was proposed in [6], establishing a UAV-based operational modal analysis approach. This method enables dynamic displacement measurement of structures using one or two cameras. Stationary or handheld cameras are often impractical for measuring structural responses due to limited accessibility or maintenance constraints; therefore, UAVs provide an effective alternative. A homography-based perspective-correction method can be applied to UAV imagery. However, traditional approaches rely on only four calibration points and suffer from signal drift. The presented study introduces, for the first time, a time-varying homography matrix computed from n calibration points to correct perspective distortion at different times, while relative displacement measurements are used to compensate for UAV planar motion. Novel contributions include the analysis and mitigation of UAV vibration effects. The proposed method was validated experimentally using a planar frame structure in laboratory conditions. Results indicate that the method effectively suppresses UAV vibrations and accurately identifies structural modal parameters. Under impulse and white-noise excitation, when $n > 60$ calibration points were used, relative errors of natural frequency and damping ratio were below 0.4% and 5.45%, respectively.

In recent years, many researchers have investigated UAV digital-twin technologies from different perspectives [7]. However, this area remains in the early stages of development, with challenges such as incomplete data and model fusion, limited algorithm migration, weak correspondence between virtual and physical domains, and insufficient application scalability. To explore the potential of digital-twin technology in

UAV applications, a digital-twin-based monocular visual-navigation framework was proposed. The framework integrates a deep-neural-network model consisting of physical, virtual, dual-data, and application layers. A multimodal decision-making model with decoupling methods was constructed at the application level, including perception and control models to study global optimal solutions and UAV behavioral control. Both the digital-twin system and the decision-making model were verified in virtual and physical environments, respectively. The results show that the proposed digital-twin-based visual-navigation system reduces algorithm development and deployment costs and enhances navigation adaptability. Compared with baseline models, the proposed decision-making model demonstrated improved navigation performance in both virtual and physical domains – approximately 8.6% higher in simulation and 2.7 times higher in real-world experiments.

UAV-based object detection aims to locate and recognize targets in aerial images, widely used for traffic monitoring, disaster response, and anomaly detection [8]. However, due to the high cost of sensors and computational constraints, deploying large, accurate multimodal detectors on UAV platforms is impractical. Inspired by model compression and cross-modal signal-processing techniques, a cross-modal knowledge-distillation detection paradigm was proposed. This approach achieves detection performance comparable to complex multimodal methods while requiring significantly fewer computational resources. Selective feature imitation is introduced to reduce redundant cross-modal feature transfer, while adaptive prediction imitation dynamically adjusts the distillation strength according to prediction quality. Large-scale experiments on an aerial vehicle dataset demonstrated improved detection performance with reduced complexity.

Minimization of energy consumption in interference-limited UAV networks was studied in [9]. The optimization problem was formulated to minimize total power subject to interference and service-quality constraints. Since the problem is non-convex, a deep-reinforcement-learning framework was employed. The proposed multimodal model integrates deep and shallow neural features to enhance prediction accuracy while maintaining computational efficiency. Simulation results indicate that the proposed algorithm outperforms existing methods.

In paper [10], a classical transfer-function approach was applied to the aircraft roll-angle automatic control system. However, the mathematical model of the controlled object and actuating mechanisms was not presented. The simulation was performed using a Simulink model.

An analysis of scientific sources [1] – [10] shows that a considerable number of studies are devoted to UAV control-system modeling, PID regulator design, navigation algorithms, modal-analysis methods, and digital-twin technologies. However, most of them lack a complete mathematical model of the controlled object or ignore the dynamic interaction within the "UAV–aileron actuator–controller" system, which complicates the synthesis of an optimal stabilization law.

Accordingly, this study addresses the scientific and practical problem of developing a UAV roll-angle stabilization system based on a full mathematical model and modal-control methods, using both an autopilot and an observer device to ensure the desired dynamic quality of the transient process. To achieve this goal, the research was conducted in the following stages.

1) Development of a complete UAV mathematical model considering moments of inertia, aerodynamic forces, and aileron-actuator dynamics.

2) Analysis of system controllability and observability.

3) Synthesis of an autopilot regulator for roll-angle stabilization using Butterworth and binomial standard forms of the characteristic equation.

4) Design of a Luenberger observer and investigation of the influence of the system's natural frequency on stabilization quality.

5) Numerical simulation of the system dynamics in MATLAB/Simulink and comparison of results for different regulator configurations and characteristic-equation forms.

The purpose of this work is to improve the efficiency and accuracy of UAV roll-angle stabilization by combining modal-analysis methods with modern approaches to regulator and state-observer synthesis. This paper has not been previously published.

II. Roll Angle Stabilization Using Autopilot

Let *Oxyz* be the coordinate system associated with the UAV as shown in Fig. 1. The equation of angular motion of the UAV relative to the longitudinal axis *Oy* is given as:

$$I\ddot{\gamma} + f\dot{\gamma} = M_y,$$

where γ is the roll angle, I is the moment of inertia of the aircraft engine relative to the longitudinal axis

Oy, *f* is the coefficient of aerodynamic drag, M_y is the moment of external forces applied to the UAV.

The equation of motion of the aileron actuator has the form [11]:

$$T\dot{\delta} + \delta = Ku,$$

where δ is the aileron deflection, T is the time constant, K is the gain, and u is the voltage supplied to the aileron drive.

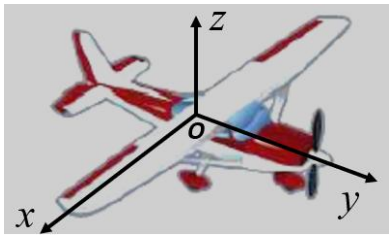

Fig. 1. Coordinate system associated with UAV

If we consider the overall dynamics of a UAV with aileron drive, then the moment of external forces applied to the UAV will depend on the aileron deflection:

$$M_y = c\delta,$$

where c is the coefficient. Thus, the mathematical model of the movement of a UAV with aileron drive will look like:

$$\begin{aligned} I\ddot{\gamma} + f\dot{\gamma} &= c\delta, \\ T\dot{\delta} + \delta &= Ku. \end{aligned} \tag{1}$$

Further, new designations were introduced:

$$x_1 = \delta, \quad x_2 = \gamma, \quad x_3 = \dot{\gamma}. \tag{2}$$

Then the equation of motion (1) in state space is:

$$\begin{aligned} \dot{\mathbf{x}} &= \mathbf{Ax} + \mathbf{Bu}, \\ \mathbf{y} &= \mathbf{Cx}, \end{aligned} \tag{3}$$

where the object matrix **A**, the control matrix **B**, and the state vector **x** have the form, if $K = c = 1$:

$$\mathbf{A} = \begin{bmatrix} -\frac{1}{T} & 0 & 0 \\ \frac{1}{I} & -\frac{f}{I} & 0 \\ 0 & 1 & 0 \end{bmatrix}, \quad \mathbf{B} = \begin{bmatrix} \frac{1}{T} \\ 0 \\ 0 \end{bmatrix}, \quad \mathbf{x} = \begin{bmatrix} x_1 \\ x_2 \\ x_3 \end{bmatrix}.$$

In the considered case, the system has one input, therefore the control vector $\mathbf{u} = u$. The controllability matrix $\mathbf{P_C} = \left[\mathbf{B} \vdots \mathbf{AB} \vdots \mathbf{A}^2\mathbf{B}\right]$ will have the form

$$\mathbf{P_C} = \begin{bmatrix} \frac{1}{T} & -\frac{1}{T^2} & \frac{1}{T^3} \\ 0 & \frac{1}{IT} & -\frac{1}{IT}\left(\frac{1}{T} + \frac{f}{I}\right) \\ 0 & 0 & \frac{1}{IT} \end{bmatrix}.$$

It is obvious that *rank* $\mathbf{P_C}$ = 3, that is, the condition of complete controllability of the system is fulfilled.

Figure 2 shows a structural diagram of a closed system with a regulator **P** [11].

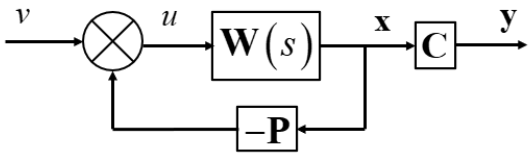

Fig. 2. Block diagram of a closed system with a regulator P

Here v is the external influence, s is the Laplace transform operator, **W**(s) is the matrix transfer function of the open system, which has the form:

$$\mathbf{W}(s) = (s\mathbf{I} - \mathbf{A})^{-1}\mathbf{B}.$$

It is easy to see that

$$u = v - \mathbf{Px}. \tag{4}$$

If we substitute the right-hand side of expression (4) into the first equation of system (3), which was previously written in the Laplace transform, we can obtain the matrix transfer function of the closed-loop system:

$$\mathbf{\Phi}(s) = (s\mathbf{I} - \mathbf{A} + \mathbf{BP})^{-1}\mathbf{B}.$$

Let $\mathbf{P} = \begin{bmatrix} p_1 & p_2 & p_3 \end{bmatrix}$. Here p_1, p_2, p_3 are the controller parameters that need to be found.

In paper [11], analytical expressions for the controller parameters are found through a laborious procedure of finding the inverse matrix $(s\mathbf{I} - \mathbf{A} + \mathbf{BP})^{-1}$. Another method was proposed in the paper. Thus:

$$s\mathbf{I} - \mathbf{A} + \mathbf{BP} = \begin{bmatrix} s + \frac{1}{T} + \frac{p_1}{T} & \frac{p_2}{T} & \frac{p_3}{T} \\ -\frac{1}{I} & s + \frac{f}{I} & 0 \\ 0 & -1 & s \end{bmatrix}. \tag{5}$$

The characteristic equation of the transfer function of a closed-loop system can be obtained through the determinant of matrix (11):

$$\det\left(s\mathbf{I}-\mathbf{A}+\mathbf{BP}\right)=s^3+\left(\frac{f}{I}+\frac{1}{T}+\frac{p_1}{T}\right)s^2+\left[\left(\frac{1}{T}+\frac{p_1}{T}\right)\frac{f}{I}+\frac{1}{I}\frac{p_2}{T}\right]s+\frac{1}{I}\frac{p_3}{T}. \quad (6)$$

Butterworth form was taken as the desired characteristic polynomial [11]:

$$H(s)=s^3+2\omega_0 s^2+2\omega_0{}^2 s+\omega_0{}^3, \quad (7)$$

where ω_0 is the natural frequency of the system.

As a result of comparing the right-hand sides of expressions (6) and (7), a system of equations was compiled, after solving which the following expressions for the controller parameters were obtained:

$$p_1=T\left[2\omega_0-\left(\frac{1}{T}+\frac{f}{I}\right)\right],$$
$$p_2=IT\left[2\omega_0\left(\omega_0-1\right)+\frac{f}{I}\right], \quad (8)$$
$$p_3=IT\omega_0^3.$$

Table I shows the roots of the characteristic equation (7) for different natural frequencies of the system. The roots of the characteristic equation are complex, which indicates the oscillatory nature of the transient process.

In the case where the autopilot is designed only to maintain a given constant bank (external signal v = 0 is absent), based on expressions (2), (4) and (8), the following autopilot equations are obtained [11]:

$$u=-\left(p_1\delta+p_2\dot{\gamma}+p_3\gamma\right). \quad (9)$$

As can be seen, the structure of equation (9) corresponds to the structure of a PID controller without an integrator. If $v \neq 0$, the first equation of system (3) can be rewritten in the form:

$$\dot{\mathbf{x}}=\left(\mathbf{A}-\mathbf{B}\cdot\mathbf{P}\right)\mathbf{x}+\mathbf{B}\cdot v. \quad (10)$$

The following parameter values were used for the calculation: I = 8.77·10 $^{-2}$ N·m·s^2 ; f = 0.12 N·m·s; T = 0.1 s. Figure 3 shows the constructed graphs of the dependence of the angle γ (Fig. 3a), angular velocity $\dot{\gamma}$ (Fig. 3b) and angle δ (Fig. 3c), which were obtained as a result of the numerical solution of equation (10): curve 1 for ω_0 = 2.65 s $^{-1}$; curve 2 for ω_0 = 4.65 s^{-1} .

TABLE I. PROBLEM SOLUTION ROOTS OF THE CHARACTERISTIC EQUATION (7)

ω_0 = 2.65 s^{-1}	ω_0 = 3.65 s^{-1}	ω_0 = 4.65 s^{-1}
–2.6500 + 0.0000i	–3.6500 + 0.0000i	–4.6500 + 0.0000i
–1.3250 + 2.2950i	–1.8250 + 3.1610i	–2.3250 + 4.0270i
–1.3250 – 2.2950i	–1.8250 – 3.1610i	–2.3250 – 4.0270i

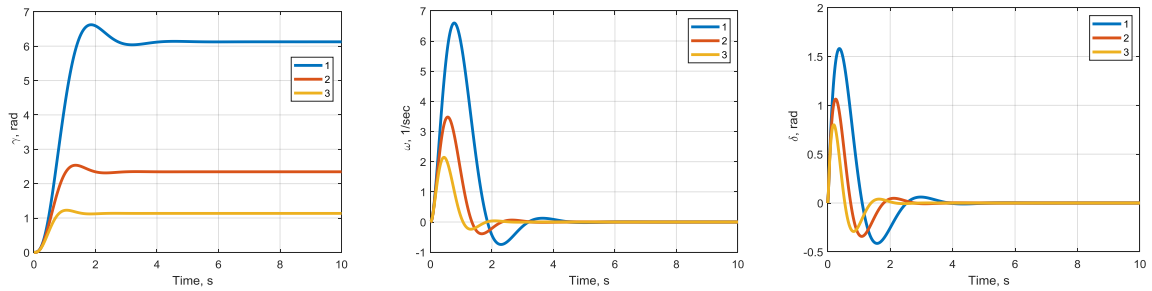

a) b) c)

Fig. 3. Dependences of angles γ, δ and angular velocity $\dot{\gamma}$ at different initial values of ω₀ obtained as a result of numerical solution of equation (10)

The solution of the differential equation (10) consists of the solution of the homogeneous equation and the steady solution. The steady solution of the differential equation (10) has the form:

$$\mathbf{x}^*=-\left(\mathbf{A}-\mathbf{B}\cdot\mathbf{P}\right)^{-1}\mathbf{B}\cdot v.$$

Therefore, for v = 1 and ω_0 = 2.65 s$^{-1,}$ the following steady-state solutions are obtained:

$$\begin{bmatrix}x_1^*\\x_2^*\\x_3^*\end{bmatrix}=-\left(\mathbf{A}-\mathbf{B}\cdot\mathbf{P}\right)^{-1}\mathbf{B}=\begin{bmatrix}0\\0\\6.127\end{bmatrix}.$$

Indeed, the graphs show that the steady-state value for the roll angle is 6.127 rad (Fig. 3a), and the steady-state values of the angular velocity $\dot{\gamma}$ (Fig. 3b) and the aileron angle δ (Fig. 3c) are zero. As can be seen, the transient process takes from 2 to 4 seconds, depending on the natural frequency of the system.

The study, in contrast to the standard Butterworth form, also considered the binomial form:

$$H(s) = s^3 + 3\omega_0 s^2 + 3\omega_0^2 s + \omega_0^3. \qquad (11)$$

As a result of comparing the right-hand sides of expressions (6) and (11), a system of equations was compiled, after solving which the following expressions for the controller parameters were obtained:

$$p_1 = T\left[3\omega_0 - \left(\frac{1}{T} + \frac{f}{I}\right)\right],$$

$$p_2 = IT\left[3\omega_0(\omega_0 - 1) + \frac{f}{I}\right],$$

$$p_3 = IT\omega_0^3.$$

system (3) can be rewritten in the form:

Table II shows the roots of the characteristic equation (11).

The obtained roots of the characteristic equation (11) indicate the aperiodic nature of the transition process. Fig. 4 shows graphs of the dependence for the angle γ (Fig. 4a), angular velocity $\dot{\gamma}$ (Fig. 4b), and angle δ (Fig. 4c): curve 1 for $\omega_0 = 2.65$ s^{-1}; curve 2 for $\omega_0 = 3.65$ s^{-1}; curve 3 for $\omega_0 = 4.65$ s^{-1}.

TABLE II. ROOTS OF THE CHARACTERISTIC EQUATION (11)

$\omega_0 = 2.65$ s^{-1}	$\omega_0 = 3.65$ s^{-1}	$\omega_0 = 4.65$ s^{-1}
–2.6500 + 0.0000i	–3.6500 + 0.0000i	–4.6500 + 0.0000i
–2.6500 - 0.0000i	–3.6500 + 0.0000i	–4.6500 + 0.0000i
–2.6500 + 0.0000i	–3.6500 - 0.0000i	–4.6500 – 0.0000i

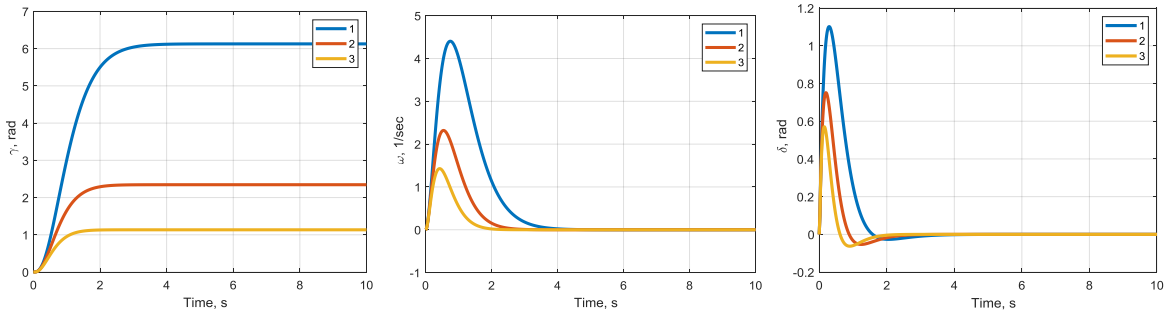

a) b) c)

Fig. 4. Dependences of angles γ, δ and angular velocity $\dot{\gamma}$ at different initial values of ω₀ obtained as a result of numerical solution of equation (10)

From the obtained results it can be seen that the transient process also takes from 2 to 4 seconds depending on the natural frequency of the system, but unlike the previous case (Fig. 3), the nature of the transient process for the roll angle is aperiodic.

III. ROLL ANGLE STABILIZATION USING OBSERVATION DEVICE

As shown in the previous study, the equations of motion (1) in state space have the form (3):

$$\dot{\mathbf{x}} = \mathbf{A}\mathbf{x} + \mathbf{B}\mathbf{u},$$

$$\mathbf{y} = \mathbf{C}\mathbf{x}.$$

The observation device according to Luinberger's law [11] has the form:

$$\dot{\hat{\mathbf{x}}} = \mathbf{A}\hat{\mathbf{x}} + \mathbf{B}\hat{\mathbf{u}} + \mathbf{K}(\mathbf{y} - \mathbf{C}\hat{\mathbf{x}}),$$

where $\hat{\mathbf{x}}$ is the state vector estimate $\mathbf{x}$; $\hat{\mathbf{u}}$ is the generated control vector; $\mathbf{K} = [k_1 \quad k_2 \quad k_3]^{\mathrm{T}}$ – matrix of gain coefficients. Passing in (12) to the Laplace transform, we obtain:

$$\hat{\mathbf{x}} = (s\mathbf{I} - \mathbf{A} + \mathbf{K}\mathbf{C})^{-1}\mathbf{B}\hat{\mathbf{u}} + (s\mathbf{I} - \mathbf{A} + \mathbf{K}\mathbf{C})^{-1}\mathbf{K}\mathbf{C}\cdot\mathbf{x}.$$

From here, the matrix transfer functions of the closed-loop system were obtained:

$$\mathbf{\Phi}_1(s) = (s\mathbf{I} - \mathbf{A} + \mathbf{K}\mathbf{C})^{-1}\mathbf{B},$$

$$\mathbf{\Phi}_2(s) = (s\mathbf{I} - \mathbf{A} + \mathbf{K}\mathbf{C})^{-1}\mathbf{K}\mathbf{C}.$$

In the case where only the roll angle is measured $\mathbf{C} = [0 \quad 0 \quad 1]$, then the observability matrix

$\mathbf{Q} = \left[\mathbf{C}^{\mathrm{T}} \vdots \mathbf{A}^{\mathrm{T}}\mathbf{C}^{\mathrm{T}} \vdots \left(\mathbf{A}^{\mathrm{T}}\right)^2 \mathbf{C}^{\mathrm{T}} \right]$ takes the following form:

$$\mathbf{Q} = \begin{bmatrix} 0 & 0 & \frac{1}{I} \\ 0 & 1 & -\frac{f}{I} \\ 1 & 0 & 0 \end{bmatrix}.$$

It is obvious that rank $Q = 3$, that is, the condition of complete observability of the system is fulfilled. Thus, we obtain:

$$s\mathbf{I} - \mathbf{A} + \mathbf{KC} = \begin{bmatrix} s + \frac{1}{T} & 0 & k_1 \\ -\frac{1}{I} & s + \frac{f}{I} & k_2 \\ 0 & -1 & s + k_3 \end{bmatrix}. \quad (13)$$

The characteristic equation of the transfer functions of the closed-loop system is obtained through the determinant of the matrix (13):

$$\det\left(s\mathbf{I} - \mathbf{A} + \mathbf{KC}\right) = s^3 + \left(\frac{f}{I} + \frac{1}{T} + k_3\right)s^2 + \left[\left(\frac{1}{T} + \frac{f}{I}\right)k_3 + k_2 + \frac{1}{T}\frac{f}{I}\right]s + \frac{1}{T}\frac{f}{I}k_3 + k_2\frac{1}{T} + \frac{1}{I}k_1. \quad (14)$$

Butterworth form (7) was taken as the desired characteristic polynomial. As a result of comparing the right-hand sides of (14) and (7), a system of equations was compiled. As a result of its solution, the following expressions for the amplification coefficients were obtained:

$$\begin{aligned} k_3 &= 2\omega_0 - \left(\frac{f}{I} + \frac{1}{T}\right), \\ k_2 &= 2\omega_0^2 - \left(\frac{f}{I} + \frac{1}{T}\right)k_3 - \frac{1}{T}\frac{f}{I}, \\ k_1 &= I\left(\omega_0^3 - \frac{1}{T}\frac{f}{I}k_3 - k_2\frac{1}{T}\right). \end{aligned} \quad (15)$$

Table III shows the roots of the characteristic equation for the standard Butterworth form (7). As can be seen, the roots of the characteristic equation are complex, which indicates the oscillatory nature of the transition process.

The equation of the error $\tilde{\mathbf{x}} = \hat{\mathbf{x}} - \mathbf{x}$ and its derivative has the following form:

$$\dot{\tilde{\mathbf{x}}} = \left(\mathbf{A} - \mathbf{KC}\right)\tilde{\mathbf{x}} + \mathbf{B}\tilde{\mathbf{u}}, \quad (16)$$

where $\tilde{\mathbf{u}} = \hat{\mathbf{u}} - \mathbf{u}$.

The following parameter values were used for the calculation: $I = 8.77 \cdot 10^{-2}$ N·m·s^2, $f = 0.12$ N·m·s, $T = 0.1$ s.

Figure 5 shows graphs of the dependence of the angle γ (Fig. 5a), angular velocity $\dot{\gamma}$ (Fig. 5b) and angle δ (Fig. 5c), which were obtained as a result of the numerical solution of equation (16) for the amplification factors (15): curve 1 for $\omega_0 = 2.65$ s^{-1}; curve 2 for $\omega_0 = 3.65$ s^{-1}; curve 3 for $\omega_0 = 4.65$ s^{1}.

TABLE III. ROOTS OF THE CHARACTERISTIC EQUATION (7)

$\omega_0 = 2.65$ s^{-1}	$\omega_0 = 3.65$ s^{-1}	$\omega_0 = 4.65$ s^{-1}
–2.6500 + 0.0000i	–3.6500 + 0.0000i	–4.6500 + 0.0000i
–1.3250 + 2.2950i	–1.8250 + 3.1610i	–2.3250 + 4.0270i
–1.3250 – 2.2950i	–1.8250 – 3.1610i	–2.3250 – 4.0270i

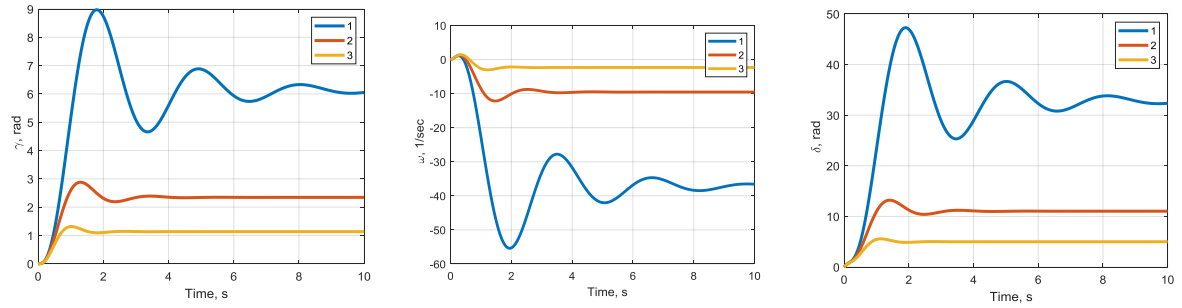

a) b) c)

Fig. 5. Dependences of angles γ, δ and angular velocity $\dot{\gamma}$ at different initial values of ω_0 obtained as a result of numerical solution of equation (16) for the amplification factors (15)

As can be seen from the obtained graphs, the transition process is oscillatory and takes more than 10 seconds, so the next stage of the study was to consider other options.

For the binomial form, the following expressions for the amplification factors are used:

$$k_3 = 3\omega_0 - \left(\frac{f}{I} + \frac{1}{T}\right),$$
$$k_2 = 3\omega_0^2 - \left(\frac{f}{I} + \frac{1}{T}\right)k_3 - \frac{1}{T}\frac{f}{I}, \quad (17)$$
$$k_1 = I\left(\omega_0^3 - \frac{1}{T}\frac{f}{I}k_3 - k_2\frac{1}{T}\right).$$

Table IV presents the roots of the characteristic equation for the binomial form for the gain coefficients (17).

The roots of the characteristic equation indicate the aperiodic nature of the transient process.

Figure 6 shows graphs of the dependence of the angle γ (Fig. 6a), angular velocity $\dot{\gamma}$ (Fig. 6b) and angle δ (Fig. 6c), which were obtained as a result of numerical solution of equation (16) for amplification factors (17): curve 1 for ω_0 = 2.65 s^{-1}; curve 2 for ω_0 = 3.65 s^{-1}; curve 3 for ω_0 = 4.65 s^{-1}.

From the results obtained, it can be seen that the transient process is similar to the transient process for the standard Butterworth form and takes from 2 to 4 seconds depending on the natural frequency of the system.

Next, the form with the following expressions for the gain coefficients was considered:

$$k_3 = 4\omega_0 - \left(\frac{f}{I} + \frac{1}{T}\right),$$
$$k_2 = 4\omega_0^2 - \left(\frac{f}{I} + \frac{1}{T}\right)k_3 - \frac{1}{T}\frac{f}{I}, \quad (18)$$
$$k_1 = I\left(\omega_0^3 - \frac{1}{T}\frac{f}{I}k_3 - k_2\frac{1}{T}\right).$$

Table V shows the roots of the characteristic equation for the binomial form for the gain coefficients (18).

The real roots of the characteristic equation indicate the aperiodic nature of the transient process. Figure 7 shows graphs of the dependence for the angle γ (Fig. 7a), angular velocity $\dot{\gamma}$ (Fig. 7b) and angle δ (Fig. 7c), obtained as a result of the numerical solution of equation (16) for the amplification factors (18): curve 1 for ω_0 = 2.65 s^{-1}; curve 2 for ω_0 = 3.65 s^{-1}; curve 3 for ω_0 = 4.65 s^{-1}.

TABLE IV. ROOTS OF THE CHARACTERISTIC EQUATION (7)

ω_0 = 2.65 s^{-1}	ω_0 = 3.65 s^{-1}	ω_0 = 4.65 s^{-1}
–2.6500 + 0.0000i	–3.6500 + 0.0000i	–4.6500 + 0.0000i
–2.6500 – 0.0000i	–3.6500 + 0.0000i	–4.6500 + 0.0000i
–2.6500 + 0.0000i	–3.6500 – 0.0000i	–4.6500 – 0.0000i

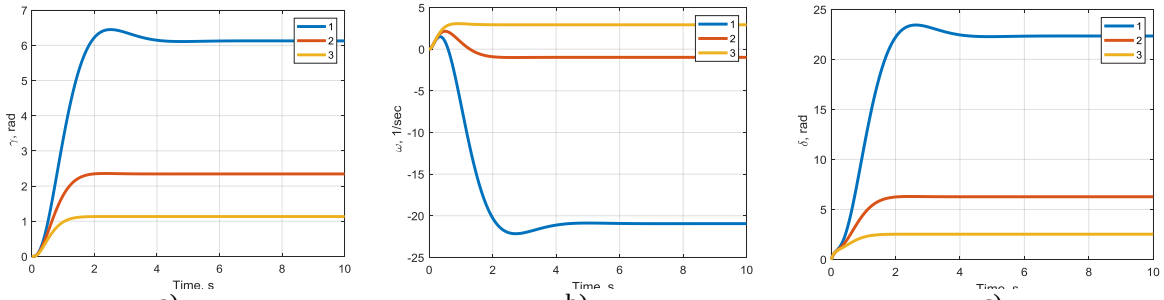

a) b) c)

Fig. 6. Dependences of angles γ, δ and angular velocity $\dot{\gamma}$ at different initial values of ω_0 obtained as a result of numerical solution of equation (16) for amplification coefficients (17)

TABLE V. ROOTS OF THE CHARACTERISTIC EQUATION

ω_0 = 2.65 s^{-1}	ω_0 = 3.65 s^{-1}	ω_0 = 4.65 s^{-1}
–6.9378	–9.5558	–12.1739
–2.6500	–3.6500	–4.6500
–1.0122	–1.3942	–1.7761

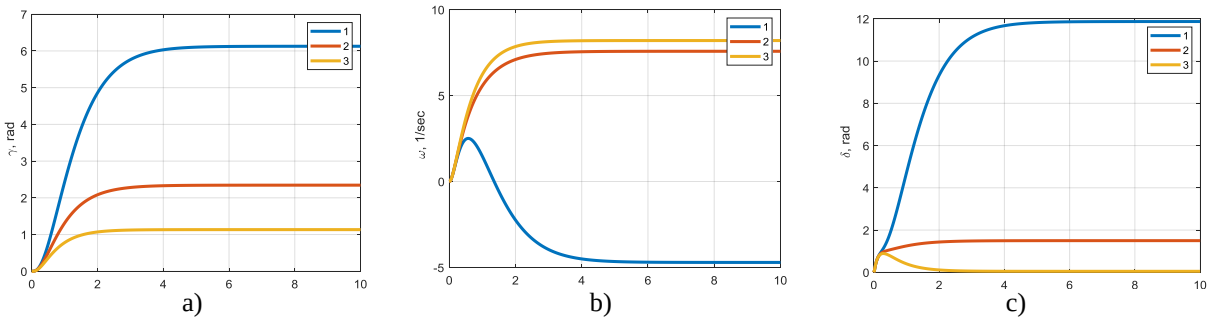

Fig. 7. Dependences of angles γ, δ and angular velocity $\dot{\gamma}$ at different initial values of ω_0 obtained as a result of numerical solution of equation (16) for amplification coefficients (18)

Analysis of the obtained results shows that the duration of the transient process, as in the previous case, is from 2 to 4 seconds depending on the value of the natural frequency of the system. At the same time, the nature of the process undergoes a qualitative change: if in the case shown in Fig. 6, oscillatory (periodic) components of the system response were observed, now the transient process has an aperiodic character for both the roll angle and the aileron rotation angle.

This means that the system reaches a steady state without oscillations around the equilibrium position, i.e. without exceeding the amplitude or phase shifts characteristic of oscillating systems. This type of transient process indicates increased damping and improved system stability, which is a desirable property for UAV attitude angle stabilization circuits.

Thus, the use of the proposed parameters of the observing device allows to provide smooth and energy-efficient control of the roll angle, reduce dynamic loads on the aileron drive and increase the accuracy of stabilization in real flight conditions. The obtained aperiodic nature of the transient process indicates the optimal agreement between the speed of the system and its stability, which confirms the effectiveness of the developed approach to modal control of UAVs.

IV. CONCLUSIONS

Based on the full mathematical model of the UAV and modal control methods, two variants of the UAV roll angle control system were considered: the first variant, an autopilot, which is built as a closed-loop automatic control system with a feedback controller, and the second - built with the help of an observer device. The conditions of controllability and observability of the UAV were analyzed . The autopilot equation was obtained, the structure of which corresponds to the structure of a PID controller. The autopilot parameters for various transient processes were obtained. Thus, the transient process for the standard Butterworth form takes from 2 to 4 seconds, depending on the natural frequency of the system. Analytical dependences of the Luinberger observer device gain coefficient matrix were obtained for various standard forms of the system characteristic equation. From the obtained results, it was established that, unlike the autopilot, the use of an observer device leads to a qualitative change in the nature of the transient process.

Thus, the use of modal control methods allows obtaining the parameters of the autopilot and the observing device for the ACS of the UAV roll angle. This approach can also be used to construct the ACS of the pitch and yaw angles not only of UAVs, but also of other types of aircraft.

REFERENCES

[1] D. A. Vadis and V. V. Avrutov, “Methods for increasing the functional efficiency of UAVs,” *Mechanics of Gyroscopic Systems*, no. 48, pp. 55–68, 2024. https://doi.org/10.20535/0203-3771482024317891

[2] Z. Kong and Q. Lu, “Mathematical Modeling and Modal Switching Control of a Novel Tiltrotor UAV,” *Journal of Robotics*, vol. 2018, no. 1, 2018, Art. no. 8641731. https://doi.org/10.1155/2018/8641731

[3] Y. Liu and H. Wang, “Mode Transition Control Law Design for a Multi-Modal UAV,” *2019 IEEE 8th Joint International Information Technology and Artificial Intelligence Conference (ITAIC)*, IEEE, 2019, pp. 1664–1671. https://doi.org/10.1109/ITAIC.2019.8785767

[4] Y. Bai, X. Li, J. Zhang, et al., “Dynamic UAV Deployment in Multi-UAV Wireless Networks: A Multi-Modal Feature-Based Deep Reinforcement Learning Approach,” *IEEE Internet of Things Journal*, 2025. https://doi.org/10.1109/JIOT.2025.3556300

[5] G. Rizzoli, F. Rebecchi, F. Biondi, et al., “Syndrone Multi-Modal UAV Dataset for Urban Scenarios,” *Proceedings of the IEEE/CVF International*

Conference on Computer Vision, 2023, pp. 2210–2220. https://doi.org/10.1109/ICCVW60793.2023.00235

[6] J. Luo, L. Zhang, Y. Chen, et al., "UAV-Based Operational Modal Analysis Method Using Improved Homography-Based Perspective Rectification Method," *Journal of Vibration and Control*, vol. 30, no. 7–8, pp. 1829–1840, 2024. https://doi.org/10.1177/10775463231171958

[7] J. Miao and P. Zhang, "UAV Visual Navigation System Based on Digital Twin," *2022 18th International Conference on Mobility, Sensing and Networking (MSN)*, IEEE, 2022, pp. 865–870. https://doi.org/10.1109/MSN57253.2022.00140

[8] A. Li, J. Chen, Z. Wang, et al., "Cross-Modal Object Detection via UAV," *IEEE Transactions on Vehicular Technology*, vol. 72, no. 8, pp. 10894–10905, 2023. https://doi.org/10.1109/TVT.2023.3262129

[9] M. A. Diallo, M. Ould-Khaoua, B. Gueye, et al., "Multi-Modal Deep Reinforcement Learning Framework for Interference-Limited RIS-Assisted UAV Wireless Network," *2025 12th IFIP International Conference on New Technologies, Mobility and Security (NTMS)*, IEEE, 2025, pp. 80–85. https://doi.org/10.1109/NTMS65597.2025.11076827

[10] R. C. Dorf and R. H. Bishop, *Modern Control Systems*, Upper Saddle River, NJ: Prentice-Hall, 2001, 831 p. https://doi.org/10.1002/acs.890

[11] B. Porter, R. Crossley, and P. A. Witting, "Modal control: Theory and applications," in IEEE Trans. Syst., Man, Cybern., vol. SMC-4, no. 6, pp. 595–596, 1974.

Received: February 09, 2026
Accepted: March 03, 2026
Published: April 19, 2026

Avrutov Vadym. ORCID 0000-0002-3875-0646. Doctor of Engineering Science. Professor.
Faculty of Robotics and Instrumentation Engineering, National Technical University of Ukraine "Igor Sikorsky Kyiv Polytechnic Institute," Kyiv, Ukraine.
Education: National Technical University of Ukraine "Igor Sikorsky Kyiv Polytechnic Institute," Kyiv, Ukraine.
Research interests: navigation systems, control systems of unmanned aerial vehicles.
Publications: 111.
E-mail: vyshgorod@gmail.com

Hehelskyi Oleksii. ORCID 0000-0002-8108-4730. Postgraduate Student.
Faculty of Robotics and Instrumentation Engineering, National Technical University of Ukraine "Igor Sikorsky Kyiv Polytechnic Institute," Kyiv, Ukraine.
Education: National Technical University of Ukraine "Igor Sikorsky Kyiv Polytechnic Institute," Kyiv, Ukraine.
Research interests: automatic control systems, UAV control.
Publications: 5.
E-mail: hehelskyi.oleksii@gmail.com

Tsisarzh Viacheslav. ORCID 0009-0004-3294-2710. Candidate of Engineering Sciences.
State Enterprise "Research Institute "Kvant-Radiolokatsiia", Kyiv, Ukraine.
Research interests: radio-location systems, control systems.
Publications: 5.
E-mail: tsisarzh_v@ukr.net

Pazdrii Olha. ORCID 0000-0002-8970-5079. Doctor of Philosophy.
Faculty of Robotics and Instrumentation Engineering, National Technical University of Ukraine "Igor Sikorsky Kyiv Polytechnic Institute", Kyiv, Ukraine
Education: National Technical University of Ukraine "Igor Sikorsky Kyiv Polytechnic Institute"
Research area: fractal analysis, non-destructive testing, vibration analysis, control systems.
Publications: 22.
E-mail: olgapazdri@gmail.com

Khutko Maksym. ORCID 0009-0006-8344-6674. Postgraduate Student.
Faculty of Robotics and Instrumentation Engineering, National Technical University of Ukraine "Igor Sikorsky Kyiv Polytechnic Institute," Kyiv, Ukraine.
Education: National Technical University of Ukraine "Igor Sikorsky Kyiv Polytechnic Institute," Kyiv, Ukraine.
Research interests: navigation systems, control systems of unmanned aerial vehicles.
E-mail: khutko.m.yu.-pg51f@edu.kpi.ua

В. В. Аврутов, О. В. Гегельський, В. В. Цісарж, О. Я. Паздрій, М. Ю. Хутко. Модальне керування кутом крену безпілотного літального апарата
У статті розглянуто задачу автоматичного керування кутом крену безпілотного літального апарата. На основі повної математичної моделі безпілотного літального апарата та методів модального керування досліджено два варіанти системи автоматичного керування: автопілот, реалізований як замкнена система зі зворотним зв'язком, та система зі спостерігаючим пристроєм. Проведено аналіз умов керованості та спостережуваності системи, отримано рівняння автопілота, структура якого відповідає ПІД-регулятору. Результати чисельного моделювання подано у вигляді часових залежностей кута крену, кутової швидкості крену та кута відхилення елерона для різних власних частот. Аналітична перевірка підтверджує значення усталеного кута крену, отриманого в результаті моделювання. Визначено параметри автопілота для різних перехідних процесів. Обчислено корені характеристичних рівнянь для стандартних біноміальної форми та форми Баттерворта, а також отримано аналітичні вирази для матриці коефіцієнтів підсилення спостерігача Люенбергера. Показано, що використання спостерігаючого пристрою суттєво змінює характер перехідного процесу системи. Запропонований підхід, заснований на методах модального керування, може бути застосований не лише для керування кутом крену, але й для синтезу систем автоматичного керування кутами тангажу та рискання як безпілотного літального апарата, так і інших літальних апаратів.
Ключові слова: автопілот, спостерігаючий пристрій, система автоматичного керування, кут крену, безпілотний літальний апарат, ПІД-регулятор.

Аврутов Вадим Вікторович. ORCID 0000-0002-3875-0646. Доктор технічних наук. Професор.
Факультет робототехніки та приладобудування, Національний технічний університет України «Київський політехнічний інститут імені Ігоря Сікорського», Київ, Україна.
Освіта: Національний технічний університет України «Київський політехнічний інститут імені Ігоря Сікорського», Київ, Україна.
Наукові інтереси: навігаційні системи, системи керування безпілотними літальними апаратами.
Кількість публікацій: 111.
E-mail: vyshgorod@gmail.com

Гегельський Олексій Володимирович. ORCID 0000-0002-8108-4730. Аспірант.
Факультет робототехніки та приладобудування, Національний технічний університет України «Київський політехнічний інститут імені Ігоря Сікорського», м. Київ, Україна.
Освіта: Національний технічний університет України «Київський політехнічний інститут імені Ігоря Сікорського», Київ, Україна.
Наукові інтереси: системи автоматичного керування, керування БПЛА.
Кількість публікацій: 5.
E-mail: hehelskyi.oleksii@gmail.com

Цисарж В'ячеслав Вікторович. ORCID 0009-0004-3294-2710. Кандидат технічних наук.
Державне підприємство «Науково-дослідний інститут «Квант-радіолокація», Київ, Україна.
Наукові інтереси: радіолокаційні системи, системи керування.
Кількість публікацій: 5.
E-mail: tsisarzh_v@ukr.net

Паздрій Ольга Ярославівна. ORCID 0000-0002-8970-5079. Доктор філософії (PhD).
Факультет робототехніки та приладобудування, Національний технічний університет України «Київський політехнічний інститут імені Ігоря Сікорського», Київ, Україна.
Освіта: Національний технічний університет України «Київський політехнічний інститут імені Ігоря Сікорського».
Наукові інтереси: фрактальний аналіз, неруйнівний контроль, вібраційний аналіз, системи керування.
Кількість публікацій: 22.
E-mail: olgapazdri@gmail.com

Хутко Максим Юрійович. ORCID 0009-0006-8344-6674. Аспірант.
Факультет робототехніки та приладобудування, Національний технічний університет України «Київський політехнічний інститут імені Ігоря Сікорського», Київ, Україна.
Освіта: Національний технічний університет України «Київський політехнічний інститут імені Ігоря Сікорського», Київ, Україна.
Наукові інтереси: навігаційні системи, системи керування безпілотними літальними апаратами.
E-mail: khutko.m.yu.-pg51f@edu.kpi.ua